VOL. 14, NO. 18, SEPTEMBER 2019 ISSN 1819-6608
ARPN Journal of Engineering and Applied Sciences

www.arpnjournals.com

NUMERICAL INVESTIGATION OF NATURAL CONVECTION IN A POROUS ENCLOSURE WITH A FLUSH MOUNTED HEATER ON THE BOTTOM WALL

Sumona Huq[1], M. M. Rahman[1], M. F. Karim[2] and M. R. Amin[2]
[1]Department of Mathematics, Bangladesh University of Engineering and Technology, Dhaka, Bangladesh
[2]Department of Mathematical and Physical Sciences, East West University, Dhaka, Bangladesh
E-Mail:fkarim@ewubd.edu/ karimfazlul67@gmail.com

ABSTRACT

In the present study, natural convection flows in a porous enclosure with a heater on the bottom wall have been investigated numerically. To change the heat transfer in the cavity, a heater is placed at different locations on the bottom wall of the cavity, while the top wall is considered to be cold and the vertical walls are kept adiabatic. The governing equations are obtained by applying the Brinkman extended Darcy flow Model and Boussinesq approximation to characterize heat flow paths along with the heat transfer rate. Finite element method is used to solve the dimensionless governing equations with the specified boundary conditions. The parameters leading the problem are the Rayleigh number (Ra), Darcy number (Da), Thermal conductivity ratio of porous media (k), Prandlt number (Pr), length and location of the heater. To observe the effects of the heater locations at various length of heater on natural convection in the cavity, three different locations of heater at bottom wall for various heater length with different values of Ra varying in the range 10^4 to 10^6 are considered. Simulated results are presented in terms of streamlines, isotherms and average Nusselt number at the hot wall in the cavity for the mentioned parameters. The results show that the length, locations of the heater and Rayleigh number have significant effect on the flow and thermal fields as well as the rate of heat transfer from the heated wall.

Keywords: Finite element method (FEM), location and length of heater, natural convection and square enclosure.

1. INTRODUCTION

The heat transfer characteristics of natural convection in a porous enclosure play an important role in the development of energy-efficient mechanical systems used in heating and cooling of the indoor environment. Natural convection in rectangular porous enclosures has been the subject of wide research in recent years. This is motivated because of the increasing interest in engineering applications, such as Petroleum reservoirs, building thermal insulation, chemical catalytic reactors, coal combustors, heat pipe technology, underground spreading of chemical waste etc [1]. Many works have been presented to explain the natural convection phenomena and heat transfer during the past few decades. Based on the systematic review, it has been found that heat transfer and fluid flow through porous media in different geometries have become interesting topic to the researchers [2]. Different types of boundary conditions were used earlier in porous enclosures or channels that have important applications in engineering, such as, filtration, separation processes in chemical industrials, solar collectors, heat exchangers, etc. Convective flow in porous media has been of great interest due to wide applications in many engineering, agricultural, geothermal, medical and biological sciences [3]. Moreover, the research on thermal convection in porous media has been conducted extensively in recent years [4,5]. Cheikh *et al.* [4] investigated the natural convection in an air-filled two-dimensional square enclosure heated with a constant source from the bottom and with different configurations of sink on other walls. Natural convection in a cavity filled with non-Darcian porous medium is numerically investigated by Beckermann *et al.* [5]. Prasad and Kulacki [6] numerically studied convection heat transfer in a rectangular porous enclosure. It is observed from their results that the heat transfer rate increases in increasing the aspect ratio. Varol *et al.* [7] numerically studied natural convection flow in a porous rectangular enclosure with a sinusoidal varying temperature profile on the bottom wall. They found that heat transfer increases with the increase of amplitude of the sinusoidal function and decreases with the increasing aspect ratio. Das and Sahoo [8] studied the effect of change of porosity on convective flow patterns. They observed that increase in porosity of the medium is found to have significant effect on the peak temperature as well as on the peak velocities. Natural convection heat transfer in a partially cooled and inclined rectangular porous enclosure had been investigated numerically by Oztop [9]. Authors found that heat transfer increases with increasing Rayleigh number and dominant parameter on heat transfer and fluid flow as well as aspect ratio. Varol *et al.* [10] studied the natural convection in a triangular enclosure with flush mounted heater on the wall.

A careful review of the above existing literature reveals that there is a lack of fundamental information regarding the flow structure and the corresponding heat transfer in partially heated and cooled porous enclosures. The main purpose of this study is to examine the effects of the heater positions, length and Rayleigh numbers on the temperature fields in both the regions of free flow and porous medium. Therefore, due to its practical interest in the engineering fields, the topic needs to be further explored. The numerical results obtained in this study are presented in terms of streamlines, isotherms and average Nusselt number at the heated wall.

The paper is organized as follows. Section 2 gives the physical configuration and the mathematical formulation. Section 3 discusses in short the numerical implementation to solve the problem while section 4 gives the code validation. Section 5 presents the result and discussion of the findings in this investigation. Finally, section 6 concludes the paper.

2. PHYSICAL CONFIGURATION AND MATHEMATICAL FORMULATION

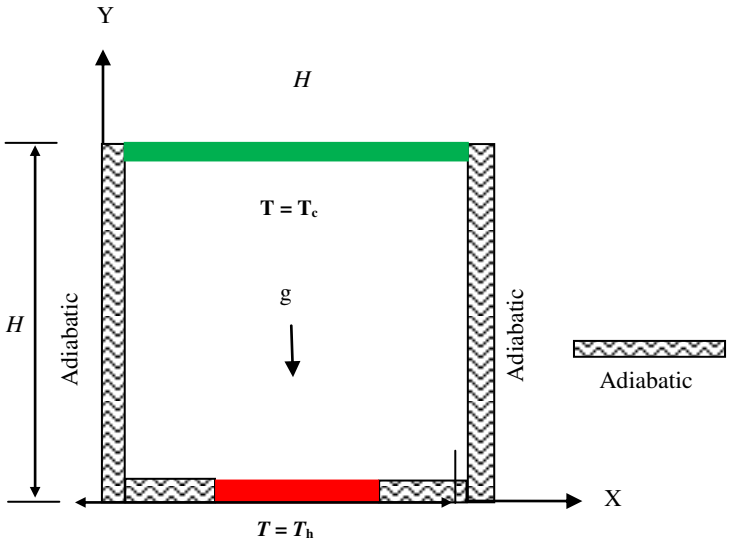

Figure-1. Schematic diagram of the physical model and boundary along with the coordinate system.

We considered a two- dimensional (2-D) square enclosure of length H filled with incompressible fluid saturated with boundary conditions and coordinates in porous medium (Figure-1). As seen from the schematic view, the top wall is cold at temperature T_c and the bottom wall is partially heated which is reserved at heat T_h, maintaining $T_h > T_c$. The remaining parts of the bottom wall and left and right walls are adiabatic. The fluid is considered as Newtonian and the fluid properties are assumed constant. The porous bed is also assumed to be uniform, isotropic and in thermodynamic equilibrium with the fluid. The Brinkman-Darcy Model has been used to solve the governing equations. According to aforesaid assumptions, the governing equations for unsteady 2-D natural convection flow in a porous enclosure using conservation of mass, momentum and energy, can be written with the following dimensionless forms:

$$\frac{\partial U}{\partial X}+\frac{\partial V}{\partial Y}=0 \quad (1)$$

$$\frac{\partial U}{\partial \tau}+U\frac{\partial U}{\partial X}+V\frac{\partial U}{\partial Y}=-\frac{\partial P}{\partial X}+\Pr\nabla^2 U-\frac{\Pr}{Da}U \quad (2)$$

$$\frac{\partial V}{\partial \tau}+U\frac{\partial V}{\partial X}+V\frac{\partial V}{\partial Y}=-\frac{\partial P}{\partial Y}+\Pr\nabla^2 V-\frac{\Pr}{Da}V+\Pr Ra\theta \quad (3)$$

$$\frac{\partial \theta}{\partial \tau}+U\frac{\partial \theta}{\partial X}+V\frac{\partial \theta}{\partial Y}=\nabla^2\theta \quad (4)$$

where, the transformed initial and boundary conditions are:

$\tau = 0$, Entire domain: $U = V = 0, \theta = 0$,

$\tau > 0$, at top wall $U = 0, V = 0, \theta = 0$

At left and right wall: $U = 0, V = 0, \frac{\partial \theta}{\partial N} = 0$.

At the bottom wall: $U = V = 0, \theta = 1$ (on the heater),

$U = 0, V = 0, \frac{\partial \theta}{\partial N} = 0$ (on the unheated part)

where N is the non-dimensional distances either along X or Y direction acting normal to the surface.

The governing equations, initial and boundary conditions are transformed into dimensionless forms using the following dimensionless variables as:

$$X=\frac{x}{H}, Y=\frac{y}{H}, U=\frac{uH}{\upsilon}, V=\frac{vH}{\upsilon}, L_h=\frac{l_h}{H}, P=\frac{pH^2}{\rho\upsilon^2}, \tau=\frac{t\upsilon}{H^2} \text{ and } \theta=\frac{T-T_c}{T_h-T_c}$$

The dimensionless parameters in the above equations, where Ra is the Rayleigh number, Pr is the Prandtl number and D_a is the Darcy number are defined

as: $$Pr=\frac{\nu}{\alpha}, Ra=\frac{\beta(T_h-T_c)H^3}{\alpha\nu}, Da=\frac{k}{H^2}$$

respectively.

The average Nusselt evaluated along the heater can be expressed as $Nu_{av}=-\frac{1}{L_h}\int_0^{L_h}\frac{\partial\theta}{\partial Y}dX$, where L_h is the length of the heater. The non-dimensional stream function is defined as: $U=\frac{\partial\psi}{\partial y}, V=-\frac{\partial\psi}{\partial x}$.

3. NUMERICAL IMPLEMENTATION

Galerkin finite element method has been used to complete discretization process of the system of partial differential equations (Equations (1)-(4)) subject to their corresponding initial and boundary conditions. The quadratic triangular element has been used to develop the finite element equations. Substitution of the obtained approximations into the system of the governing equations and boundary conditions yield a residual for each of the conservation equations. These residuals are reduced to zero in a weighted sense over each element volume using the Galerkin method. Details of the method are available in Zienkiewicz and Taylor work [13].

4. CODE VALIDATION

A comparison of streamlines and isotherms between Bhuvaneswari *et al.*[1]and present study for Gr = 10^6, Ar= 3, ε = 0.2 and Da = 10 is presented in Fig. 2. This figure shows that agreement between the present study and Ref. [1] is fairly reasonable.

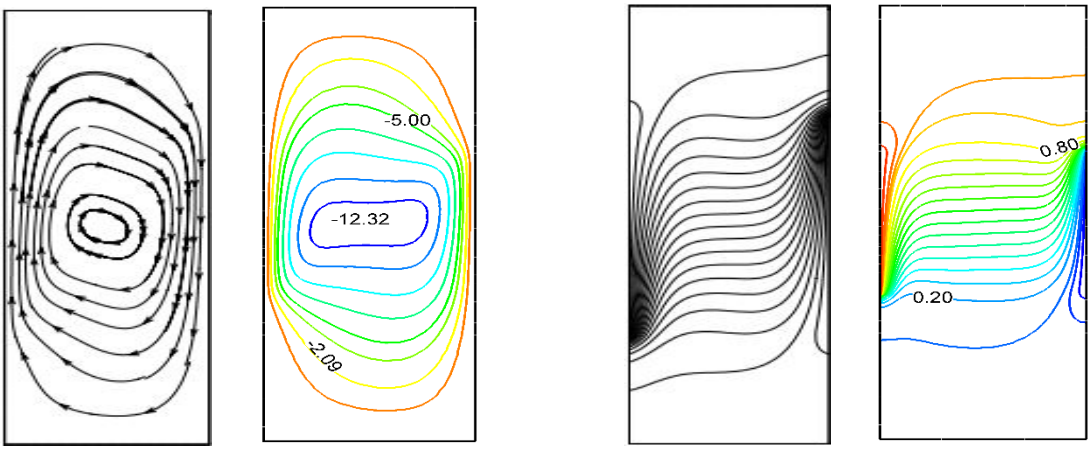

Figure-2. Streamlines (left) and isotherms (right) for Middle–Middle heating locationwith Gr =10^6, Ar = 3, ε = 0.2 and Da = 10^{-3}.

5. RESULT AND DISCUSSIONS

In the present study, 2-D laminar natural convection heat transfer and fluid flow are considered in a square enclosure for different dimensionless parameters; heater length, heater position and Rayleigh number. Position of heater is tested for the following three cases: left position (*L*p), middle position (*M*p) and right position (*R*p) of the bottom wall for three different heater lengths L_h = 0.2, 0.4, 0.6 with Rayleigh number from 10^4 to 10^6. In this study, Darcy number, Da =10^{-3} , and the ratio of the thermal conductivity of solid to fluid of porous media similar to [12] is chosen to be k = 0.0082 with Prandtl number is fixed at 0.7. The streamlines, isotherms, average Nusselt number at the hot wall in the cavity are plotted with partially heated wall for different aforesaid parameters.

5.1 ISOTHERMS AND STREAMLINES FOR LENGTH L_1= 0.2

The location of heater is a significant parameter on natural convection as indicated by Varol *et al.* [10]. Figures 3 and 4 shows the isotherm contour for three different positions of the heater of fixed length with Rayleigh numbers at τ = 0.1 and τ = 1, while length L_l = 0.2 is fixed for left (*L*p), middle (*M*p) and right (*R*p) position. It is observed from the figures that fluid rises from the center of the heater for small length of heater at bottom wall due to buoyancy for all the three positions. At time τ = 0.1, a smooth, parabolic temperature distribution is observed for the lowest values of Ra (= 10^4) for the aforesaid locations of the heater (Figure-3). However, with the increasing of Rayleigh number, up to 10^6, it remains no longer parabolic and becomes nonlinear for all aforementioned locations of the heater due to the strong buoyancy effect. It is also observed that for Ra = 10^6, temperature rises from the center of the heater and then spreaded around along top cold wall for all positions and two small circulating vortices are situated at the left and right top corner for the position *Mp* and a single circulating vortex is set at the right top corner for *Lp* and the isotherm pattern of position *Lp* is a mirror image of *Rp* for all Ra at both time τ = 0.1 and τ = 1 (as shown in Figures 3, 4).

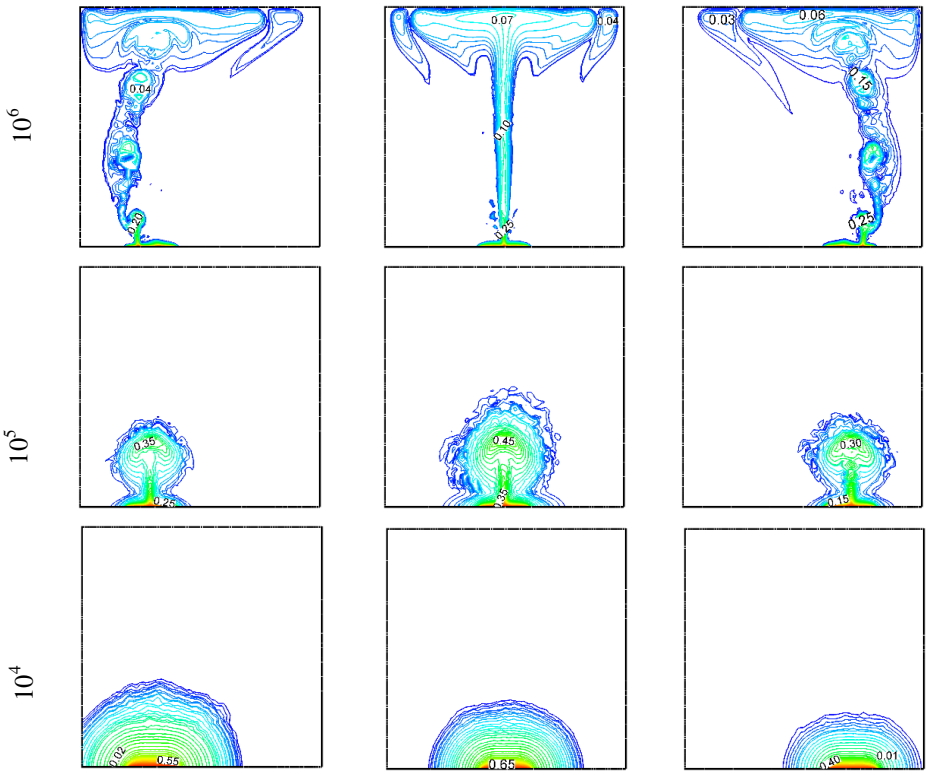

Figure-3. Isotherm contours with various Rayleigh number for various position of a heater for length L_l= 0.2 with position (a) *L*p, (b) *M*p, (c) *R*p at τ = 0.1.

It is also observed from Figure-4 that heat distribution increases with increasing of the dimensionless time τ = 1. A smooth balloon shape temperature distribution is observed for lower *Ra* for all aforesaid position of the heater. With the increasing of *Ra* to 10^5, it becomes nonlinear and spreads along the top cold wall for all aforementioned locations of the heater. Further, as *Ra* increases up to 10^6, the nonlinearity in the isotherms becomes higher and mushroom-shaped temperature distribution is observed due to the durable effect of temperature difference for all positions. As increases time, from τ = 0.1 to τ = 1, the temperature is distributed from left to right for *Lp* and from right to left for *Rp* in the enclosure and intensified along the cold wall of the enclosure. This is because, at the highest Rayleigh number, natural convection is more effective than that of the conduction of the porous medium.

Figures 5 and 6 demonstrate the stream line contour for different positions of the heater at the bottom wall at τ = 0.1and 1 with the mentioned value of *Ra*, while L_l= 0.2 is fixed for left (*L*p), middle (*M*p) and right (*R*p) position. It can be seen from Figure-5 that clockwise and anti-clockwise flows are shown via negative and positive signs of stream functions for all positions at τ = 0.1. For the lower value of *Ra* (= 10^4) the pattern of the counter rotating circulations is almost identical and the contour values of the core region are also same for all different locations of the heater. Two counter rotating symmetric cells with respect to a symmetric line are observed for the position *Mp* for all *Ra*. For *Ra* = 10^5, flow patterns are almost similar as *Ra* = 10^4 and the flow strength increases and becomes nonlinear for higher values of *Ra* due to the effect of temperature difference. It can also be seen from the Figure-5 that three small anti-clockwise rotating cells and two clockwise rotating cells are observed in the cavity for position *Lp* for *Ra* = 10^6 and also observed that the flow pattern of the position *Lp* is a mirror image of the position *Rp* for all *Ra*.

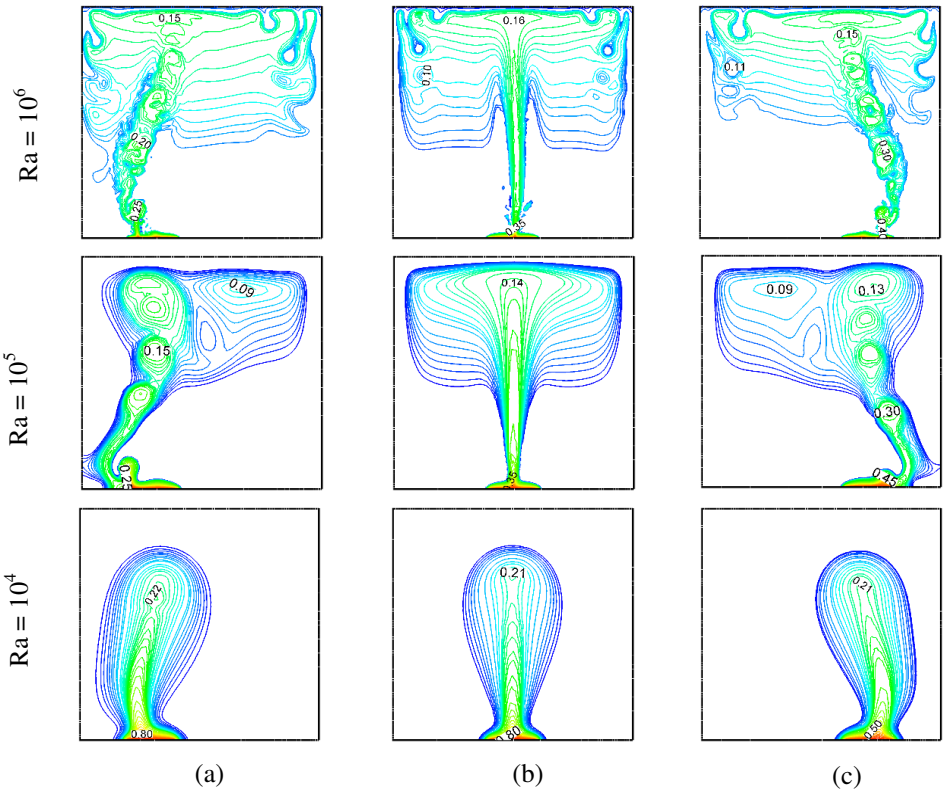

Figure-4. Isotherm contours with various Rayleigh number for various position of a heater for length $L_1 = 0.2$ with position (a) *L*p, (b) *M*p, (c) *R*p at $\tau = 1$.

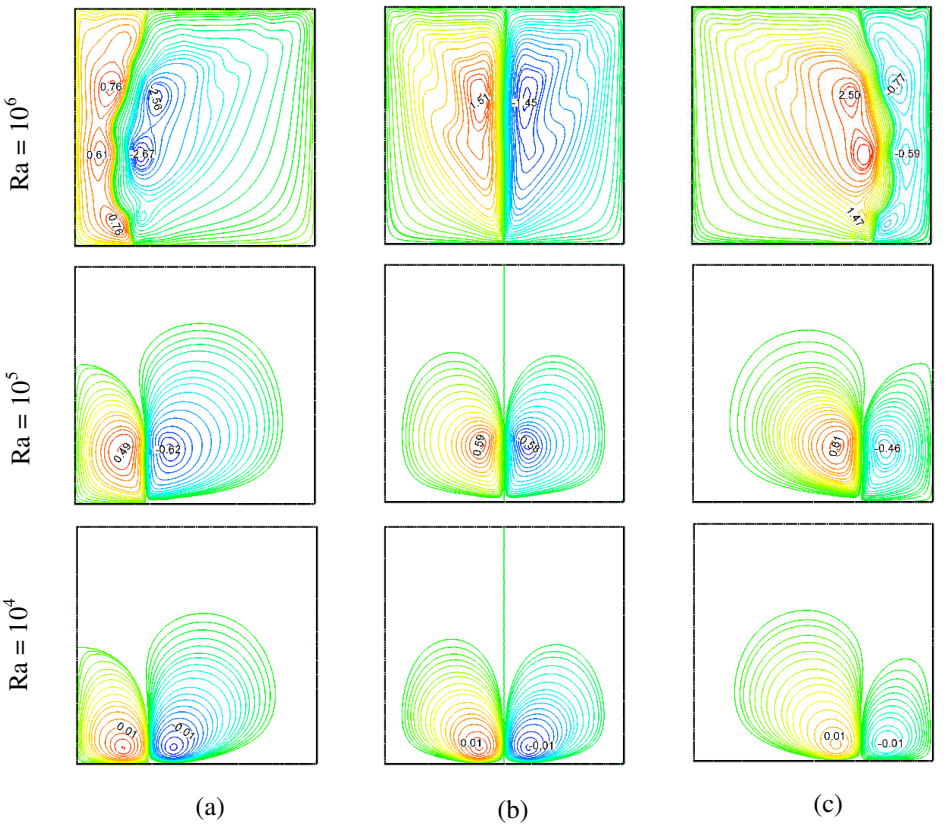

Figure-5. Streamline contours with various Rayleigh number for various position of a heater for length $L_1 = 0.2$ with position (a) *L*p, (b) *M*p, (c) *R*p at $\tau = 0.1$.

From Figure-6, it is seen that flow strength increases with increasing of the dimensionless time $\tau = 1$. Here, it is shown that for small length of heater at the bottom wall and cold top wall, flow field forms symmetric rolls with clockwise and anti-clockwise rotations inside the cavity. The patterns of the streamlines are almost similar for different positions. It is observed that for $Ra = 10^4$ at*L*p position,a smooth and symmetric anti-clockwise vortex and clockwise vortex are divided into two small vortices in the core region and the flow pattern of *Rp* is a mirror image of *Lp*. This indicates that conduction is the mode of the heat transfer. As increasing *Ra* up to 10^6, multiple number of small vortices are shown in the cavity for positions *Lp* and *Rp*. The flow intensity increases as *Ra* increases and the elliptic shaped circulation cell becomes more elliptic for the position *Mp*. The values of the stream functions at the core of the symmetric rolls increases and becomes more nonlinear with increasing the Rayleigh number for all the three positions due to the strong buoyancy effect generated by the temperature difference.

5.2 ISOTHERMS AND STREAMLINES FOR LENGTH $L_2 = 0.4$

Figures 7 and 8 show the thermal field for three different positions of the heater with Rayleigh numbers at $\tau = 0.1$ and $\tau = 1$, while length $L_2 = 0.4$ is fixed for left (*L*p), middle (*M*p) and right (*R*p) position. It is observed from Figure-7 that fluid temperature rises from the heater and a smooth one-headed almost parabolic shaped thermal lines are shown near the heater due to increase the heated surface (from 0.2 to 0.4) for all three positions for the lowest value of *Ra* (= 10^4). With the increasing of Rayleigh number up to 10^5, it turns into two headed balloon shaped thermal lines and becomes nonlinear for all aforementioned locations of the heater due to the high temperature effect. It is also observed that for $Ra = 10^6$, temperature rises from the heater then it spreads about symmetrical with vertical direction (heated to cold top wall) and becomes more nonlinear for all aforesaid positions due to strong buoyancy effect.

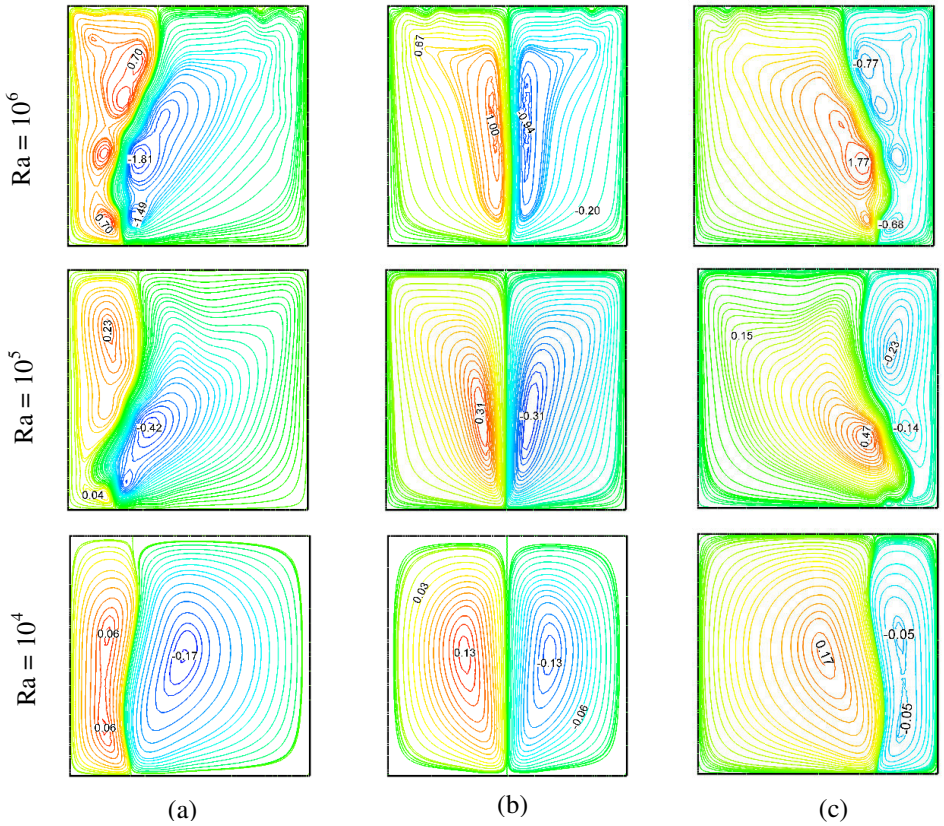

Figure-6. Stream Line contours with various Rayleigh number for various position of a heater for length $L_1 = 0.2$ with position (a) *L*p, (b) *M*p, (c) *R*p at $\tau = 1$.

It is observed from Figure-8 that heat distribution increases with increasing the dimensionless time $\tau = 1$. It is shown that the isotherm patterns of various positions of a heater for length $L_1 = 0.2$ at $\tau = 1$ (Figure-4) is almost similar for length $L_2 = 0.4$ at $\tau = 1$ (Figure-8). However, the heat distribution intensity and contour value are increased with increasing the value of *Ra* due to increase of the length of the heated surface for the all aforesaid positions as shown in Figure-8. It can also be seen that heat is distributed from the heater as several rotating cells and nonlinearly explored along the top cold wall for higher *Ra* due to strong buoyancy effect in the porous enclosure. Figures 9 and 10 illustrate the streamline contour for three different positions of the heater at bottom wall at $\tau = 0.1$ and 1 with the mentioned value of *Ra*, while $L_2 = 0.4$ is fixed for left (*L*p), middle (*M*p) and right (*R*p) position. It

can be seen from the Figure-9 that the clockwise and anti-clockwise flows are via negative and positive signs of stream functions for all different positions at $\tau = 0.1$. For the lower value of *Ra* (= 10^4) the pattern of the counter rotating circulations is almost identical and the contour value of the core regions are also same for all these different locations of the heater. This also indicates that conduction is the mode of heat transfer. It is seen that stream lines are composed of counter rotating circulating multiple cells due to the increase the length of the heater for all the positions at $Ra = 10^5$ and also observed that the flow pattern of the position *Lp* is a mirror image of the position *Rp* for all *Ra*. It can also be seen that the flow strength becomes nonlinear with multiple cells and spreads along the whole cavity for higher value of *Ra* due to the effect of natural convection for all the mentioned positions at bottom wall.

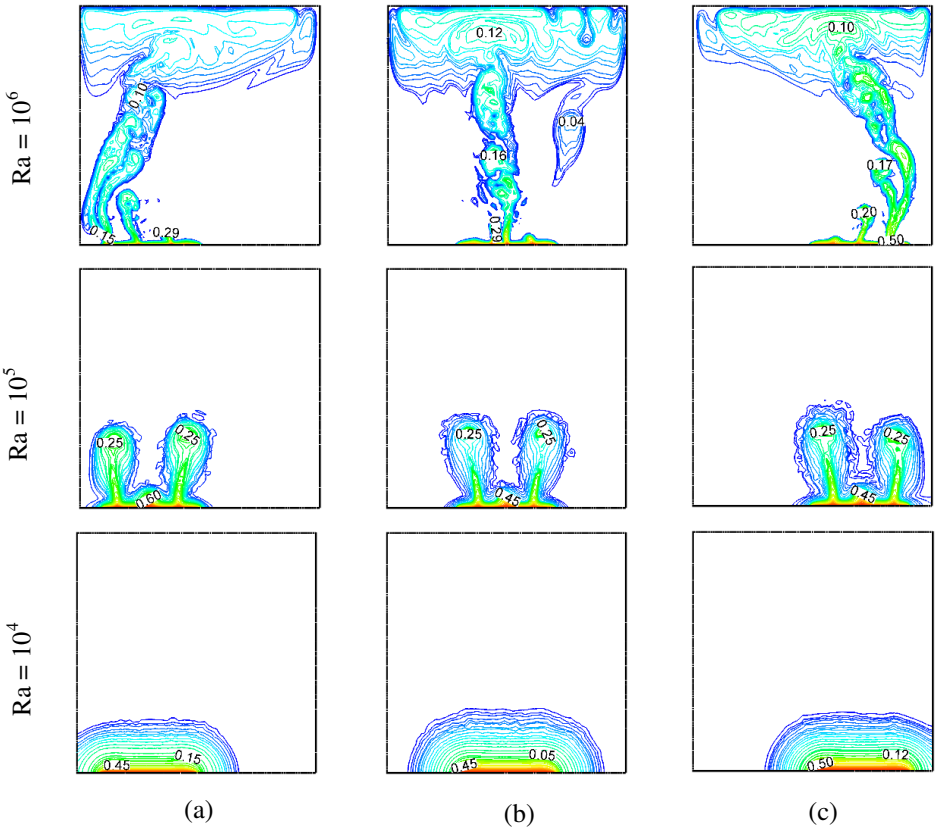

Figure-7. Isotherm contours with various Rayleigh number for various position of a heater for length L_2= 0.4 with position (a) *L*p, (b) *M*p, (c) *R*p at $\tau = 0.1$.

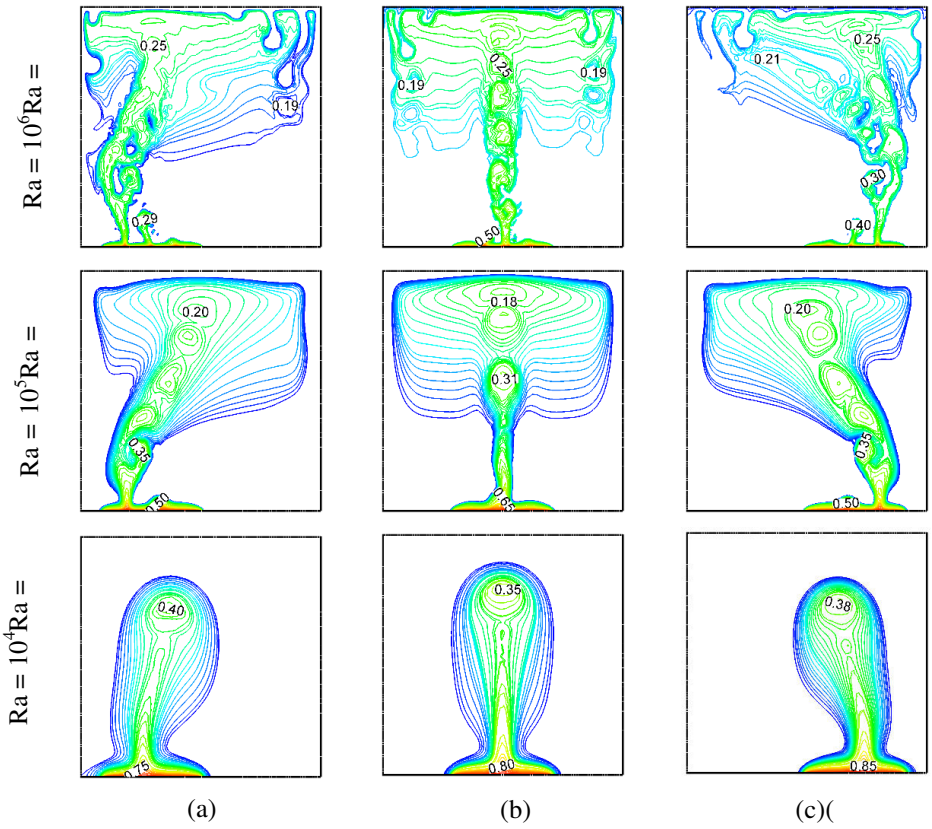

Figure-8. Isotherm contours with various Rayleigh number for various position of a heater for length L_2= 0.4 with position (a) *L*p, (b) *M*p, (c) *R*p at $\tau = 1$

It is observed from Figure-10 that flow intensity increases with increasing of time $\tau = 1$. It is shown that the flow patterns of various positions of a heater for length $L_1 = 0.2$ at $\tau = 1$ (Figure-6) is almost identical of various positions for length $L_2 = 0.4$ at $\tau = 1$ (Figure-10). However, the flow intensity and the contour value of the core region are increased with increasing the value of *Ra* due to increase of the length of the heated surface for all the aforesaid positions.

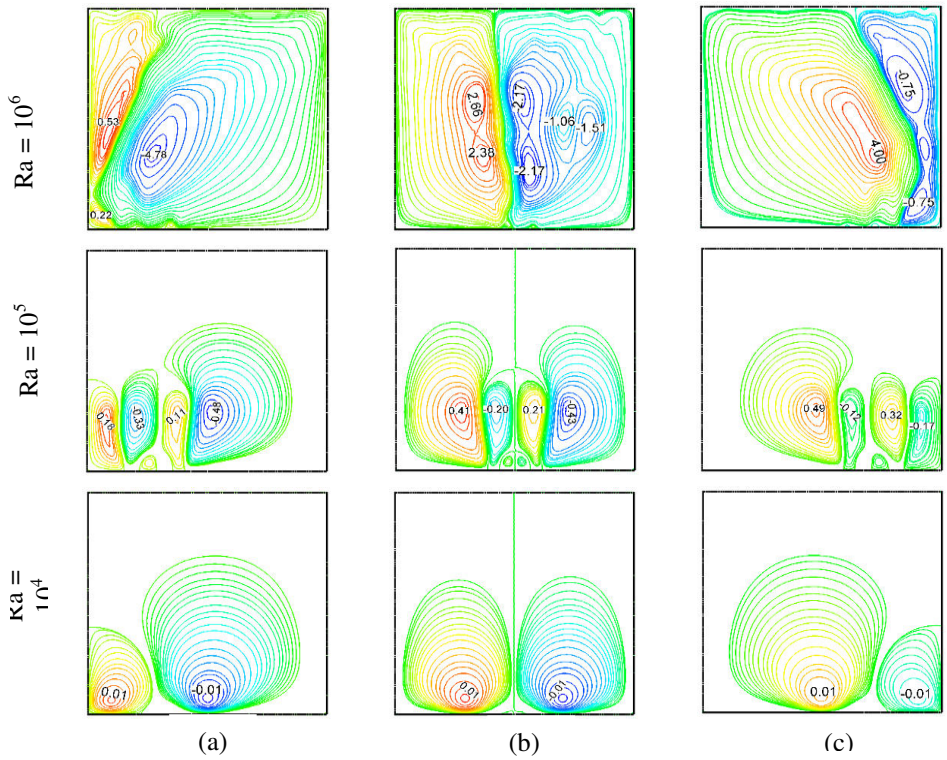

Figure-9. Stream Line contours with various Rayleigh number for various position of a heater for length L_2= 0.4 with position (a) *L*p, (b) *M*p, (c) *R*p at τ = 0.1.

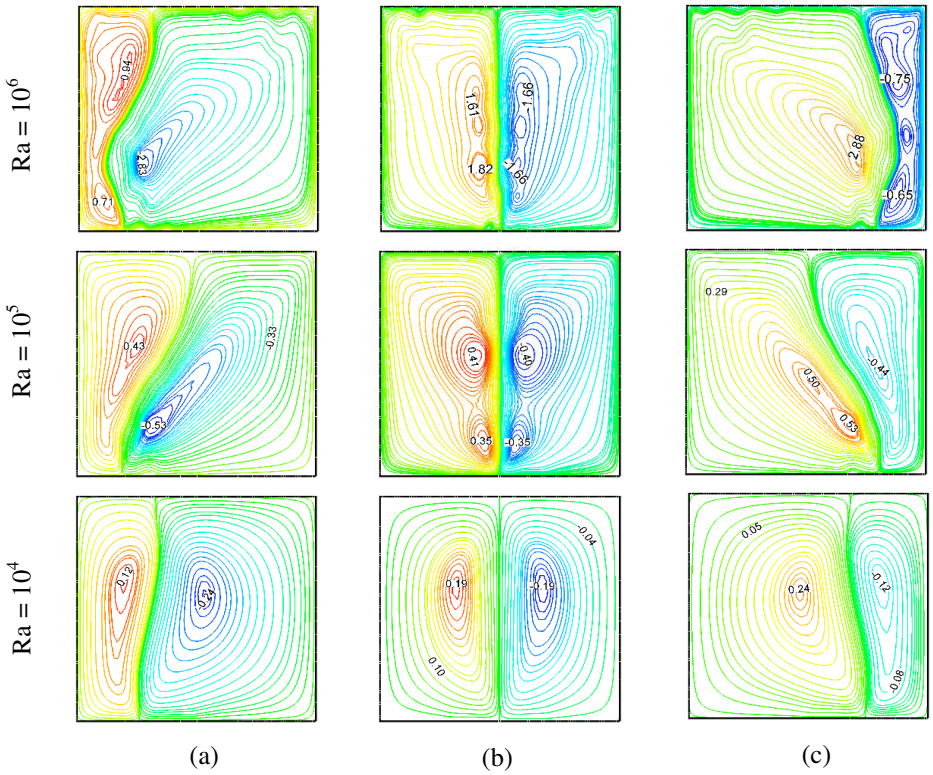

Figure-10. Stream Line contours with various Rayleigh number for various position of a heater for length L_2 = 0.4 with position (a) *L*p, (b) *M*p, (c) *R*p at τ = 1.

5.3 ISOTHERMS AND STREAMLINES FOR LENGTH L_3 = 0.6:

Figures 11-12 show the thermal field for three different positions of the heater at the bottom wall with the mentioned value of *Ra* at τ = 0.1 and τ = 1, while length L_3= 0.6 is fixed for the aforementioned positions. It is observed from Figure-11 that fluid temperature rises from the heater and a smooth almost parallel shaped thermal lines are shown near the heater for all the three positions for the lowest value of *Ra* (= 10^4). The isothermal lines are almost parallel to the bottom wall due to the increase of the length of the heated surface (from 0.2 to 0.6). With increasing the Rayleigh number up to 10^5, it becomes nonlinear and heat distributes parallelly from left side of the heater and rises upward from the right side of the heater then turn back to the bottom wall for *Lp* locations of the heater are observed and heat distribution patterns of *Rp* is inverse pattern of *Lp* for the all mentioned locations. Two headed balloon shaped heat distribution patterns are also observed for *Mp* location of the heater for *Ra* = 10^5.It is also detected that for *Ra* = 10^6, temperature rises from the heater then it spreads up with vertical direction (heated to cold top wall) then spreads along cold top wall and becomes more nonlinear for all the aforesaid positions, indicating well established natural convection heat transfer in the porous cavity.

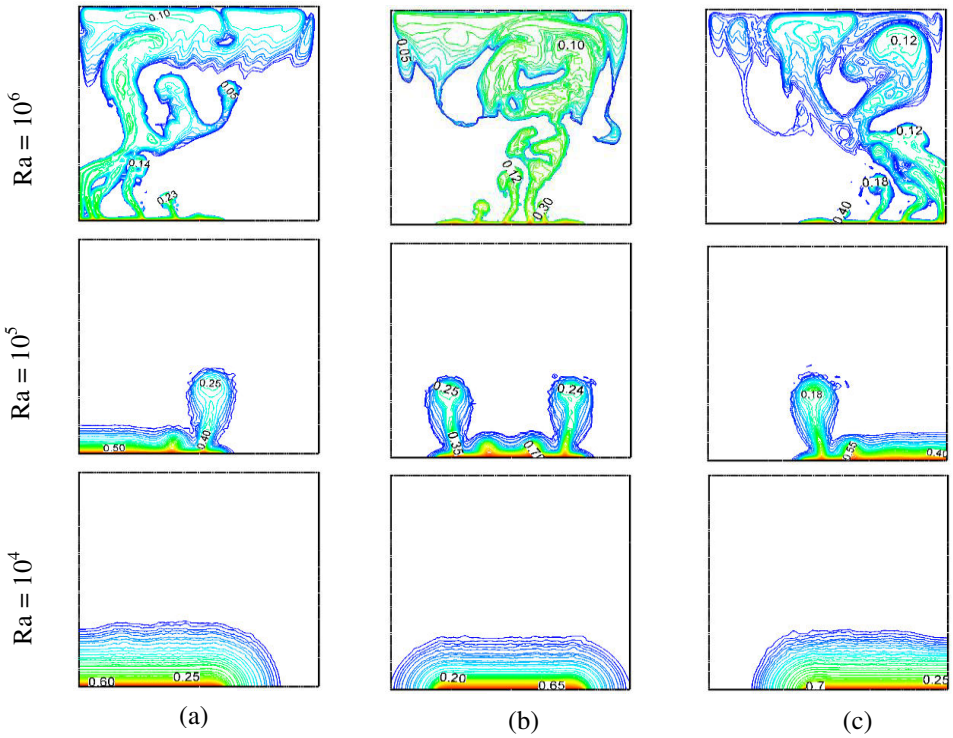

Figure-11. Isotherm contours with various Rayleigh number for various position of a heater for length L_3 = 0.6 with position (a) *L*p, (b) *M*p, (c) *R*p at τ = 0.1.

From Figure-12, it is observed that heat distribution increases with increasing of dimensionless time τ = 1.It can be seen that with the increase of heater length (from 0.2 and 0.4 to 0.6) higher isotherms patterns can be observed atτ = 1. Thermal lines are spreaded from left to right for the position *Lp* of the heater and from right to left for the position *Rp* of the heater. It is observed that for *Ra* = 10^4, isotherm patterns are smooth two headed balloon shaped for all mentioned locations. With the increase of *Ra,* it remains no longer smooth and spreads nonlinearly along the top wall. It is also detected that few small vortices are produced on the heater for higher value of *Ra*. This happens due to the generation of high heat transfer rates as the length of heat source increases. It is noticed that the heater length has a direct influence on the thermal field. With the increase in heater length, the temperature levels of isotherms increase and they become more stratified.

Figures 13 and 14 illustrate the flow field for three different positions of the heater at the bottom wall at τ = 0.1 and 1 with the mentioned value of *Ra*, while L_3= 0.6 is fixed for all positions. It can be seen from the Fig. 13 that at *Ra* = 10^4, clockwise and anti-clockwise flows with respect to a symmetric line are shown via negative and positive signs of stream functions for *Mp* positions and a single clockwise and anti-clockwise rotating cell is observed near the heater for the positions *Lp* and *Rp* respectively at τ = 0.1. This is because of increasing of the heater length. With the increase of *Ra* to10^5, streamlines are composed of counter rotating multiple cells are observed for *Mp* position and counter rotating two cells are observed for *Lp* and *Rp* positions and these are almost half of the cavity. It can also be seen that the flow strength becomes nonlinear with multiple cells and spreads along the whole cavity for higher value of *Ra* due to the effect of

buoyancy force in the porous medium for all the mentioned positions at the bottom wall.

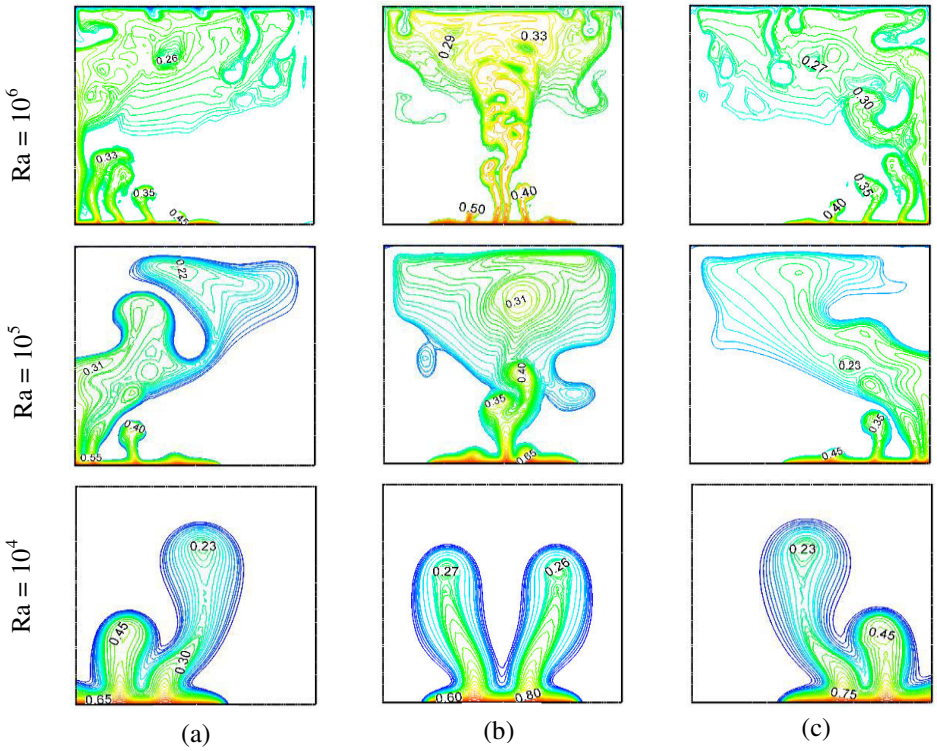

Figure-12. Isotherm contours with various Rayleigh number for various position of a heater for length $L_3 = 0.6$ with position (a) *L*p, (b) *M*p, (c) *R*p at $\tau = 1$.

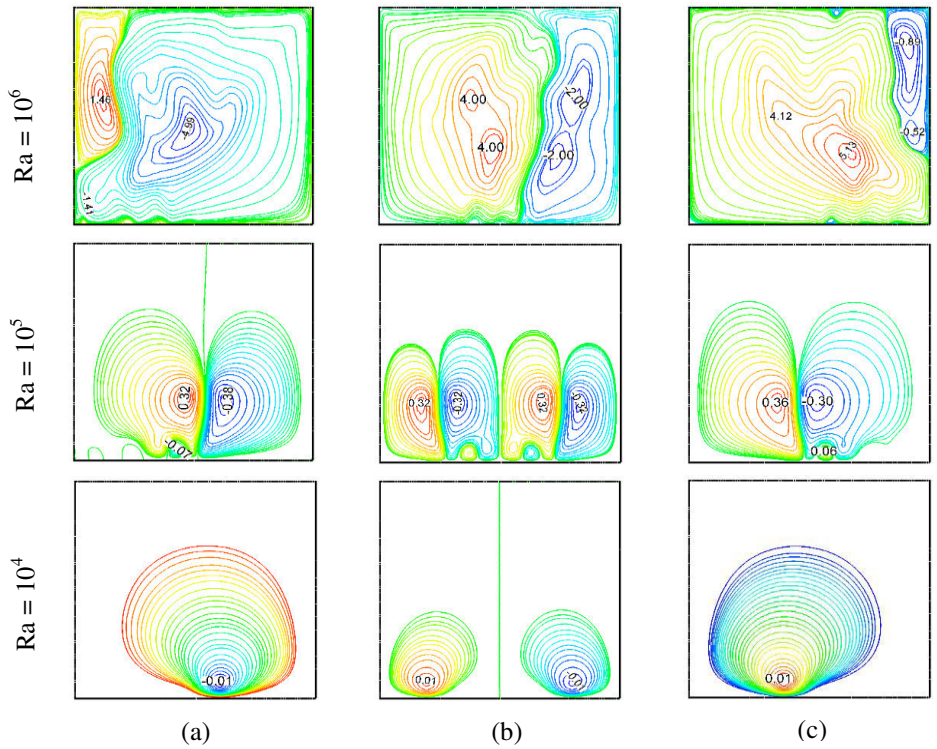

Figure-13. Stream Line contours with various Rayleigh number for various position of a heater for length $L_3 = 0.6$ with position (a) *L*p, (b) *M*p, (c) *R*p at $\tau = 0.1$.

From Figure-14, it is observed that flow strength increases with increasing the value of *Ra* and dimensionless time $\tau = 1$. It can be seen from the figure that clockwise and anti-clockwise flows are shown via negative and positive signs of stream functions for all positions. Multiple cells are observed for position *Mp*, and the position *Lp* has two anti-clockwise rotating cells and a large clockwise rotating cell. The flow pattern of *Lp* is a mirror image of *Rp* for all mentioned *Ra*. This is due to increasing the heater length. As *Ra* increases up to10^5, anti-clockwise cells are small in size and are observed at the left-top corner in the cavity for the position *Lp* and multiple cells are reduced to two large cells with few small vortices in the core region within the whole cavity are observed for *Mp* position due to the slightly increase the temperature difference. It can also be seen that the flow strength becomes nonlinear for higher value of *Ra* and small vortices are almost vanish for the position *Mp* and a small anti-clockwise flow is observed at the left-top corner in the cavity for the position *Lp* and the right-top corner for *Rp* due to the strong effect of the buoyancy force in the porous medium for all the mentioned positions at the bottom wall. It is noticed that the heater length has a direct influence on the flow field.

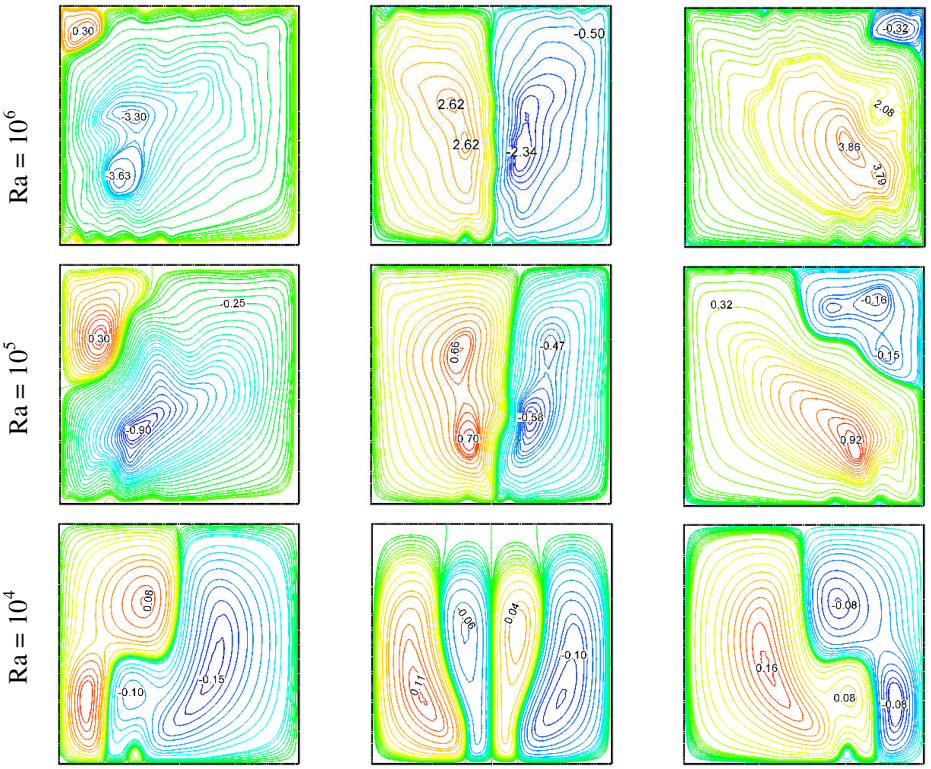

Figure-14. Stream Line contours with various Rayleigh number for various position of a heater for length $L_3 = 0.6$ with position (a) *L*p, (b) *M*p, (c) *R*p at $\tau = 1$.

The variations of the average Nusselt number with the Rayleigh number for different lengths of the heater in different positions (left, middle and right) with respect to time are presented in Figures 15-17. It is seen from Figure-15 that the average heat transfer rate gives higher value for small length of the heater at $Ra = 10^4$ for all the mentioned positions. That is, the average Nusselt number is minimum with the increase of the heater length for all the aforesaid positions for lower value of *Ra*. Wave like behavior near the side wall appears for all mentioned positions, as time is increased.

Figure-16 depicts the variation of the average Nusselt number at the heated surface in the cavity for different heater lengths with respect to time indifferent locations of the heater at $Ra = 10^5$. It is noticed that for the length 0.2 at the *Lp* position, the slope shows negativity from initial stage to more than half time of the process, then it increases with time and shows almost similar characteristics with other lengths to the end of the process. For larger values of the heater length (0.4, 0.6), it has been found that the slope shows positivity from initial stage with the slight increase of the heater length. The average Nusselt number changes little with time for the heater length 0.4 and 0.6. From this figure, it is observed that when the heater is located at *Lp* and *Rp* positions, they show almost similar characteristics. When heater is located at the middle-position (*Mp*), the length $L_1 = 0.2$ gives almost constant value of the average Nusselt number and little change is observed for the higher length (0.4, 0.6) with respect to time.

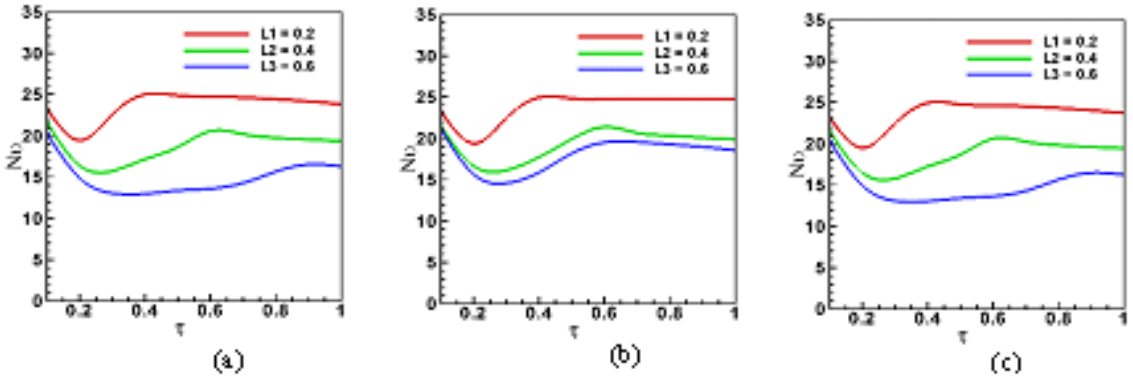

Figure-15. Variation of average Nusselt number for different length of heater at $Ra = 10^4$ with different position of heater at (a) *Lp*, (b) *Mp* and (c) *Rp*.

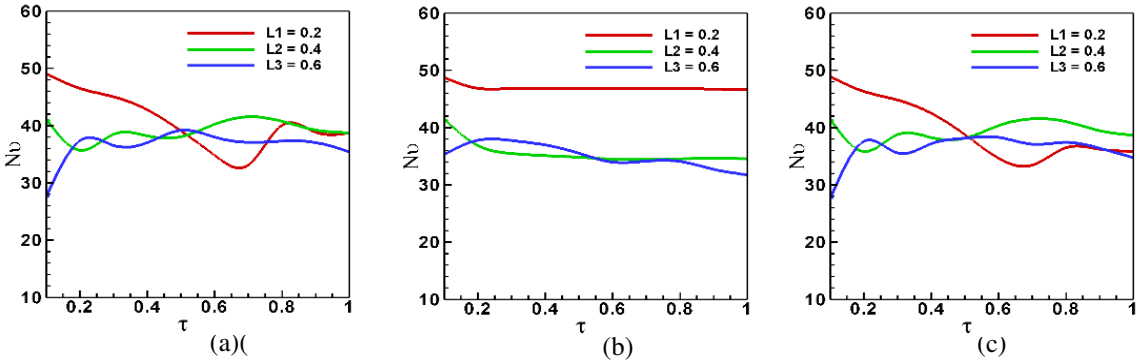

Figure-16. Variation of average Nusselt number for different length of heater at $Ra = 10^5$ with different position of heater at (a) *Lp*, (b) *Mp* and (c) *Rp*.

Figure-17 depicts the variation of the average Nusselt number at the heated surface in the cavity for different heater lengths with respect to time in different locations of the heater at $Ra = 10^6$. From this figure, it is noticed that the slope shows negativity from initial stage to the end of the process with respect to time and the length of the heater shows almost similar characteristics with each other. On the other hand, the average Nusselt number is minimum with the increasing of the heater length for positions *Lp* and *Rp*. for higher values of *Ra* with respect to time. The value of average Nusselt number gives maximum value for length from 0.6 to 0.2at initial period. Conversely, with increasing time slightly the value of the average Nusselt number gives maximum value for length from 0.2 to 0.6. Meanwhile, it is seen that the average heat transfer rate increases with increasing the Rayleigh number at the stated value of heater length. It is noticed that the heater length has a direct impact on the average heat transfer rate for different length of the heater at the bottom wall. With the increase in the heater length, the heat transfer rate increases and it becomes more stratified.

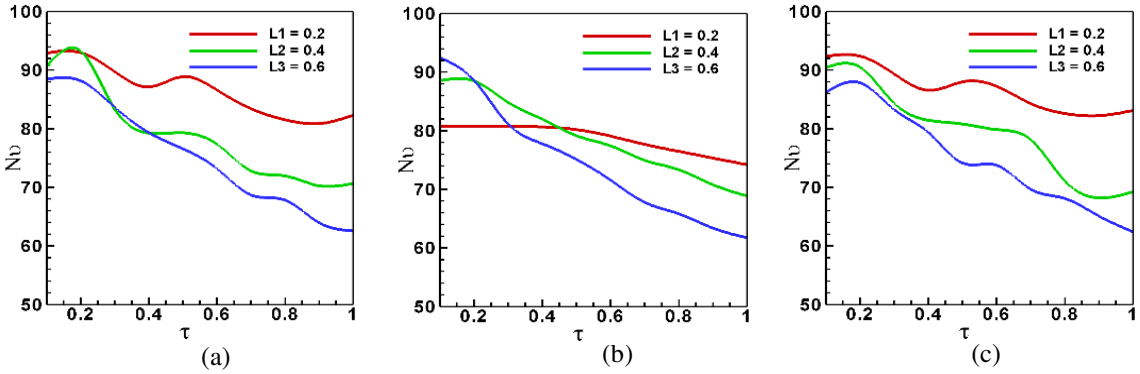

Figure-17. Variation of average Nusselt number for different length of heater at $Ra = 10^6$ with different position of heater at (a) *Lp*, (b) *Mp* and (c) *Rp*.

6. NOMENCLATURE

Da	Darcy number	*Lp*	heater at left position
Pr	Prandtl number	*Mp*	heater at middle position
Ra	Rayleigh number	*Rp*	heater at right position
Nu	Average Nusselt number	*Greek symbols*	
K	Thermal conductivity ratio	*A*	thermal diffusivity
H	length of the cavity	*B*	thermal expansion coefficient
L_h	Length of the heater	*M*	dynamic viscosity
T	Temperature	*N*	kinematic viscosity
P	dimensional pressure	θ	non-dimensional temperature
P	non-dimensional pressure	ρ	density
T	dimensional time	Ψ	stream function
G	gravitational acceleration	*T*	dimensionless time
x, y	dimensional coordinates	*Subscripts*	
X, Y	dimensionless coordinates	*Av*	average
u, v	dimensional velocity components	*H*	hot
U, V	dimensionless velocity components	*C*	cold

7. CONCLUSIONS

A computational work has been done using finite element method to investigate the unsteady natural convection flow and heat transfer in a square porous enclosure with a flush mounted heater.

The following conclusions can be drawn on the basis of the discussions:

a) The size and position of the heater has a profound impact on the heat transfer rate. Flow and temperature fields are affected by the length, location of the heater and the Rayleigh number. When the heater is located at the middle of the wall, the average Nusselt number at the hot wall in the cavity becomes higher for the Rayleigh number considered.

b) Fluids flow and heat transfer characteristics inside the porous cavity strongly depend upon the length of the heater. The average Nusselt number at the hot wall becomes higher for the lower values of the heater length at the considered Rayleigh number.

c) Nusselt number increases with the increase of *Ra* while the Nusselt number decreases with time. Wave like behavior near the side wall appears. It is also observed that Nusselt number decreases with the increase of the heater length and this implies that convection plays a significant role in the heat transfer process.

REFFERENCE

[1] M. Bhuvaneswari, S. Sivasankaran and Y. J. Kim. 2011. Effect of aspect ratio on convection in a porous enclosure with partially active thermal

walls.Computers and Mathematics with Applications. 62, 3844-3856.

[2] K. Vafai. 2005. Handbook of porous media. 2nd Edition, Taylor & Francis, New York.

[3] D. A. Nield and A. Bejan. 2013. Convection in porous media. 4th Edition, Springer Science and Business Media, NewYork. 778.

[4] N. B. Cheikh, B. B. Beya and T. Lili. 2007. Influence of thermal boundary conditions on natural convection in a square enclosure partially heated from below.Int. Comm. Heat Mass Transfer. 34, 369-379.

[5] C. Beckermann, R. Viskanta and S. Ramadhyani. 1986. A numerical study of non-Darcian natural convection in a vertical enclosure filled with a porous medium.Numer. Heat Transfer A. 10, 557-570.

[6] V. Prasad and F. A. Kulacki. 1984. Connective heat transfer in a rectangular porous cavity - Effect of aspect ratio on flow structure and heat transfer.J. Heat Transfer. 106, 158-165.

[7] Y. Varol, H. F. Öztop and I. Pop. 2008. Numerical analysis of natural convection for a porous rectangular enclosure with sinusoidal, varying temperature profile on the bottom wall.Int. Comm. Heat Mass Transfer. 35, 56-64.

[8] S. Das and R. K. Sahoo. 1999. Effect of Darcy, fluid Rayleigh and heat generation parameters on natural convection in a porous square enclosure: a Brinkman extended Darcy model.Int. Comm. Heat Mass Transfer. 26, 569-578.

[9] H. F. Öztop. 2007. Natural convection in partially cooled and inclined porous rectangular enclosures.Int. J. Therm. Sci.46, 149-156.

[10] Y. Varol, A. Koca and H. F. Öztop. 2006. Natural convection in a triangular enclosure with flush mounted heater on the wall.Int. Comm. in Heat and Mass Transfer. 33, 951-958.

[11] M. M. Rahman, M. A. H. Mamun, M. M. Billah and R. Saidur. 2010. Natural convection flow in a square cavity with internal heat generation and a flush mounted heater on a sidewall.J. of Naval Architecture and Marine Engineering.7, 37-50.

[12] W. Woodside. 1958. Calculation of the thermal conductivity of porous media.Can. J. Phys. 36, 815.

[13] O. C. Zienkiewicz and R. L. Taylor. 2005. The finite element method Solid and Structural Mechanics.Sixth Ed., McGraw-Hill.